SUPPORTING APPENDIX FOR

High-resolution cryo-EM structure of photosystem II from the mesophilic cyanobacterium, *Synechocystis* sp. PCC 6803

Christopher J. Gisriel[a], Jimin Wang[b], Jinchan Liu[b], David A. Flesher[b], Krystle M. Reiss[a], Hao-Li Huang[a], Ke R. Yang[a], William H. Armstrong[c,†], M. R. Gunner[d], Victor S. Batista[a], Richard J. Debus[e], and Gary W. Brudvig[a,b,*]

[a]Department of Chemistry, Yale University, New Haven, CT 06520, USA.
[b]Department of Molecular Biophysics and Biochemistry, Yale University, New Haven, CT 06520, USA.
[c]Department of Chemistry, Boston College, Chestnut Hill, MA 02467, USA.
[d]Department of Physics, City College of New York, New York, NY 100031, USA.
[e]Department of Biochemistry, University of California, Riverside, CA 92521, USA.
[†]Retired
*To whom correspondence should be addressed: gary.brudvig@yale.edu

Supplementary Texts

Text S1. Comparison of Ca-binding sites.

Calcium is an important nutrient in photosynthetic metabolism and is known to stabilize PSII, impacting oxygen evolution, photoprotection, and photoactivation (1–3), suggesting important biological relevance to its presence in molecular structures of PSII. The cryo-EM structure of PSII from *Synechocystis* 6803 contains three unique Ca-binding sites in addition to the Ca ion in the OEC. One is found buried in the interface between PsbU and the lumenal domain of CP47, another is partially solvent-exposed between PsbV and the lumenal domain of CP43, and a third is found in a solvent-exposed region near PsbK, Psb30, and CP43 (**Fig. S7**). Other than the Ca found in the OEC, no Ca-binding sites were assigned in the *T. vulcanus* PSII cryo-EM structure (4), but various Ca-binding sites were assigned in the XRD structure of PSII from *T. vulcanus* (5). It is noteworthy that Ca-containing salt was included in the sample buffer used for the *Synechocystis* 6803 PSII cryo-EM sample preparation described herein and in the crystallization buffer used for the *T. vulcanus* PSII XRD structure (5), but none was included in the sample buffer used for the *T. vulcanus* PSII cryo-EM structure (4). In the XRD structure of PSII from *T. vulcanus*, three Ca-binding sites are located on the lumenal side of each PSII monomer, and one additional Ca ion is assigned on the stromal side of only one monomer (5). The Ca ion on the stromal side is involved in crystal contacts, and is thus unlikely to be biologically relevant. Unlike the buried Ca-binding sites observed in *Synechocystis* 6803 PSII, all three other Ca ions in the *T. vulcanus* PSII XRD structure are found in highly solvent-accessible peripheral regions: one is near the dimeric interface, another is on the outside of PsbO whose possible role in proton ejection has been discussed previously (6, 7), and a third is nearby PsbV and PsbF. These observations suggest that Ca-binding sites are variable between mesophilic and thermophilic cyanobacteria, and that these sites are titratable, requiring the inclusion of Ca in the sample buffer to maintain their occupancy that may be important for stabilization of the complex. The significance of the unique Ca-binding sites in *Synechocystis* 6803 PSII discussed here are unclear, but their identification allows for future experimentation to explore their functional roles in PSII.

Text S2. PsbQ-binding.

The overall structure of PsbQ in *Synechocystis* 6803 PSII is similar to the previously-reported XRD structures (8, 9) (**Table S5**). The N-terminus is known to be covalently-linked to a lipid *in vivo* (10), and although the cryo-EM structure has much of the N-terminus resolved, sidechains of the first few modeled residues are unclear likely due to its flexibility. Of all the subunits in the PSII structure, PsbQ is located in the region of lowest resolution, and requires a lower map threshold for its visualization. Furthermore, map sharpening convolutes its ESP, being much better resolved in the unsharpened map (**Fig. S8**). These observations suggest that PsbQ is only partially occupied in the isolated PSII and may also imply low stability compared to the other extrinsic subunits.

Because PsbQ is present in the *Synechocystis* 6803 PSII structure but not in structures of *T. vulcanus* PSII, we wanted to better understand the intermolecular forces that drive binding. In plants and algae, a lumenal loop of CP43 is inserted into a helical break of PsbQ (11), a motif that is also present in the *Synechocystis* 6803 PSII structure. Nearby this loop insertion, the indole nitrogen of a CP43-Trp residue donates a H-bond to the backbone carbonyl of a PsbQ Gly residue (**Fig. S9** and **Fig. S10**), which is also observed in *Synechocystis* 6803 PSII. *T. vulcanus* also maintains these CP43 features, yet PsbQ is not bound in the reported structures. To understand what molecular interactions additionally contribute to PsbQ-binding, we performed PsbQ docking calculations on *Synechocystis* 6803 and *T. vulcanus* PSII, maintaining the restraint of the conserved CP43-Phe/PsbQ-Gly proximity (see ***Materials and Methods***). In both cases, a binding coefficient set that favors electrostatic interactions gave the lowest energy model clusters (**Table S6**), suggesting that PsbQ-binding in *Synechocystis* 6803 is primarily driven by electrostatic forces. We note that the free energy calculated by ClusPro corresponds to the PIPER energy which does not include entropic contributions, so the reported value should not be taken as the true binding energy, but is instead useful for a qualitative comparison of binding affinity (12). The calculated PIPER energy associated with PsbQ-binding in *Synechocystis* 6803 was lower than that of *T. vulcanus*; therefore, we identified residues that provide electrostatic interactions between PsbQ and the rest of the complex in the *Synechocystis* 6803 PSII structure (**Fig. 2*C***) and compared their sequence conservation in PSII from other organisms (**Fig. 2*D***). In the *Synechocystis* 6803 PSII structure, four residues from PsbQ appear to form electrostatic interactions with other PSII subunits: the sidechains of Arg83, Arg84, Glu113 and Arg122. These interact with the sidechains of CP43-Glu91, CP43-Asp182, CP43-Arg184, and PsbO-Asp38, respectively. None of the PsbQ residues found to be interacting in the *Synechocystis* 6803 PSII structure are conserved in the PsbQ sequences from *T. vulcanus* or *T. elongatus*, but many are conserved in the PsbQ homologs from plants and algae (**Fig. 2*D***). We conclude that although PsbQ-binding is driven by electrostatic interactions in cyanobacteria, those interactions are weaker in thermophilic cyanobacteria. It is plausible that salt routinely used in preparation buffers causes the dissociation of PsbQ from the complex in mesophilic and thermophilic cyanobacterial PSII, albeit more so in the latter.

Text S3. DFT calculations of Mulliken spin densities for Mn ions in the OEC.

To assess the valence states of Mn ions in the *Synechocystis* 6803 PSII cryo-EM structure, we ran single point DFT calculations of the OEC and its surrounding residues (see ***Materials and Methods***), whose nuclei are fixed in the position of the input model. These single point DFT calculations produced the Mulliken spin density for each Mn atom, whose absolute value corresponds to the number of unpaired electrons in the outermost orbital (3d). Thus, the absolute value of the Mulliken spin density 5, 4, and 3 correspond to Mn ions in oxidation states II, III, and IV, respectively. For the first and second initial guess, we set the four Mn atoms (Mn1-Mn4) in oxidation states III, IV, IV, and III, respectively, where the first guess was set to a high spin state (S=7) and the second and third guesses were set to a low spin state (S=0). For the third initial guess, we set all of the Mn ions in oxidation state II and changed the O5 ligand to a water molecule due to the long Mn-Mn and Mn-O distances (see **Table S9**). All three initial guesses resulted in Mulliken spin densities with absolute values between 5 and 4 corresponding to Mn in oxidation states II and III (**Table S7**). Because a high oxidation state model of the OEC requires Mn ions in oxidation states ≥3, these calculations support the hypothesis that the Mn ions experience electron beam-induced reduction during data collection.

Supplementary Figures

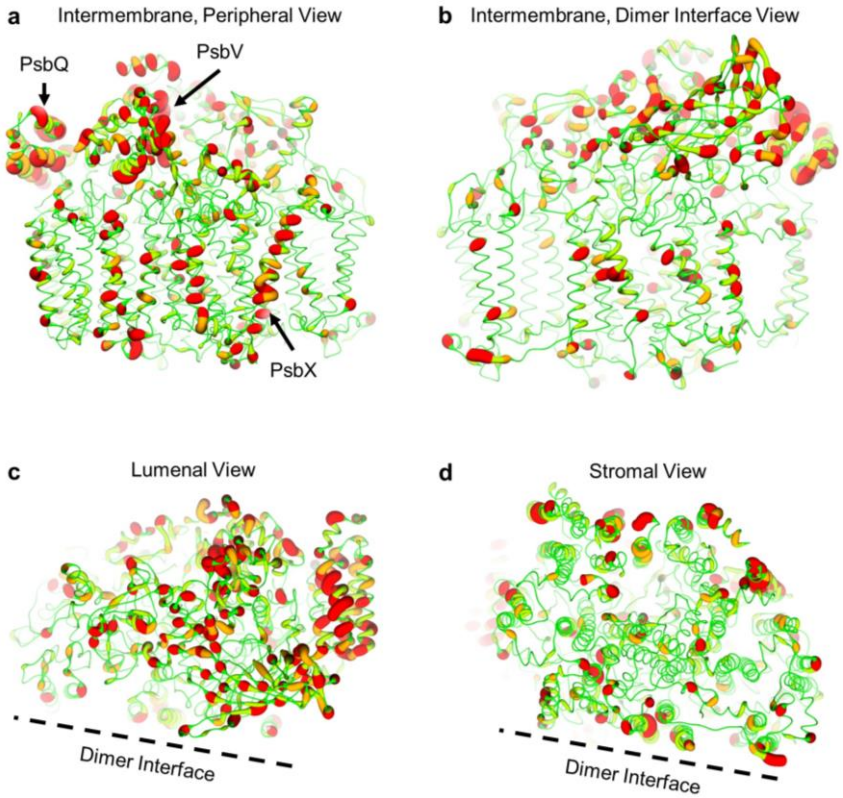

Fig. S1. Structural depiction of sequence similarity comparing PSII subunits from *Synechocystis* 6803 and *T. vulcanus*. Only the polypeptides are shown for a monomer of the *Synechocystis* 6803 cryo-EM structure in four views (**a-d**) as labeled, and the ribbons are sized and colored according to sequence similarity with *T. vulcanus* from thin green (high similarity) to thick red (low similarity). On panel **a**, subunits whose sequence identity is <50% (**Table S1**) are labeled. On panels **c** and **d**, the dimer interface is labeled.

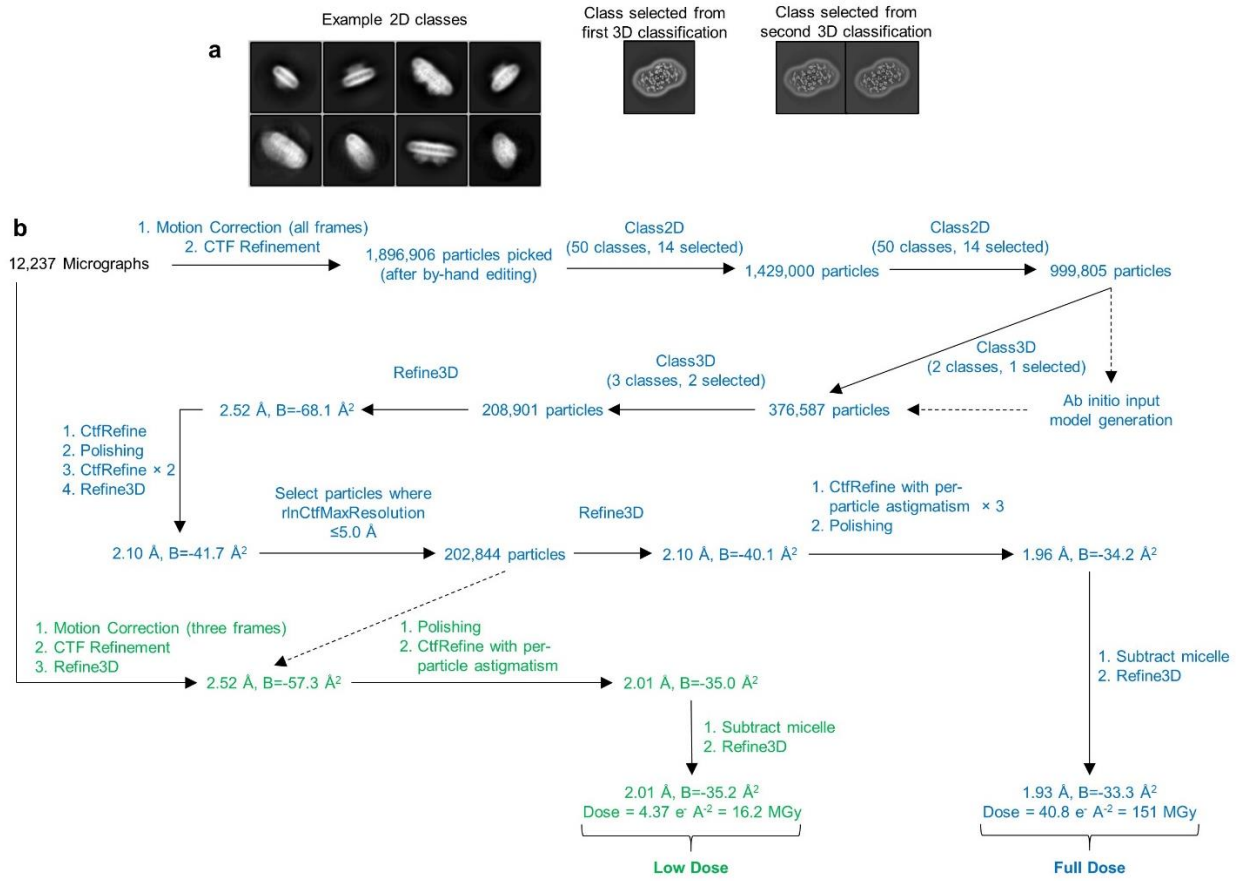

Fig. S2. Data processing of *Synechocystis* 6803 PSII structures. **a.** Representative 2D Class Averages and slices through selected 3D Class Averages. **b.** Workflow of data processing using Relion 3.1 (13).

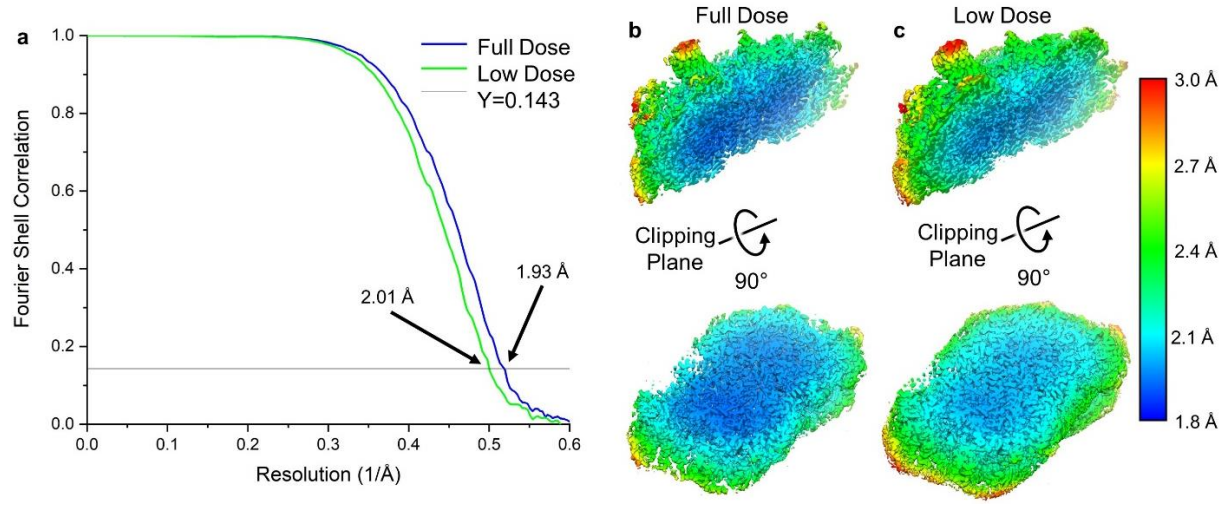

Fig. S3. Resolution of *Synechocystis* 6803 PSII structures. **a.** FSC curves for the full dose and low dose structures. **b.** Local resolution maps for the full dose and low dose structures. In **b**, the unsharpened maps are shown for both structures. The clipping plane is shown parallel to the membrane plane on the long axis of the structure (top) and parallel to the membrane plane (bottom). Local resolution values are represented by colors shown in the scale bar. Local resolution was calculated using Relion 3.1's implementation of LocRes (13).

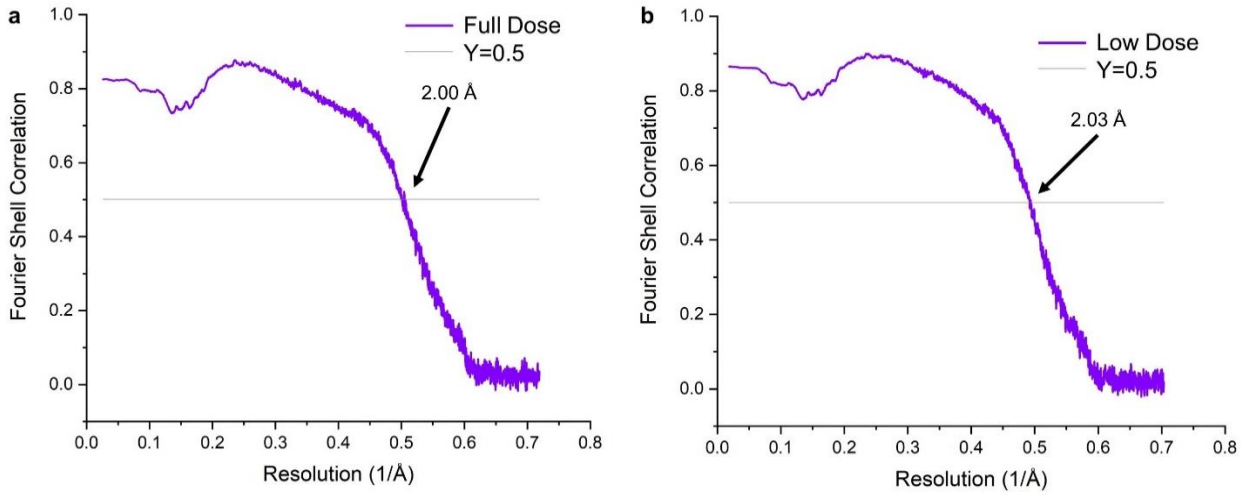

Fig. S4. Map-to-model FSCs of full dose and low dose maps. **a.** Map-to-model FSC curve for the full dose structure. **b.** Map-to-model FSC curve for the low dose structure. Curves were generated using the Phenix software suite (14).

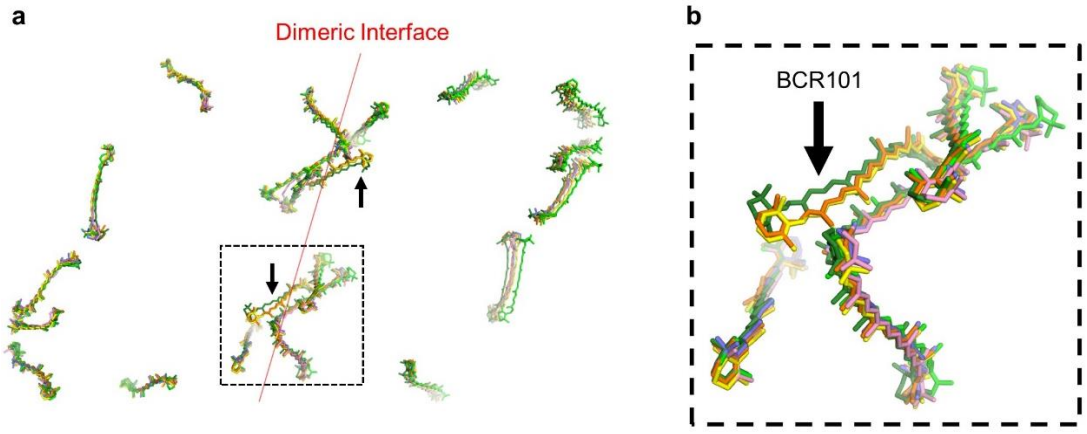

Fig. S5. Lack of carotenoid 101 in *Synechocystis* 6803 PSII. **a.** A lumenal view of core-associated carotenoids is shown from various PSII structures. The dimeric interface is shown as a red line and the carotenoid 101 site is designated with an arrow. **b.** Enlarged boxed region from **a**. In both panels, PSII models are shown from *Synechocystis* 6803 (blue, PDB 7N8O), *T. vulcanus* (orange, PDB 7D1T), *T. elongatus* (yellow, PDB 6W1O), *P. sativum* (dark green, PDB 5XNL), *C. reinhardtii* (bright green, PDB 6KAC), and *C. caldarium* (pink, PDB 4YUU).

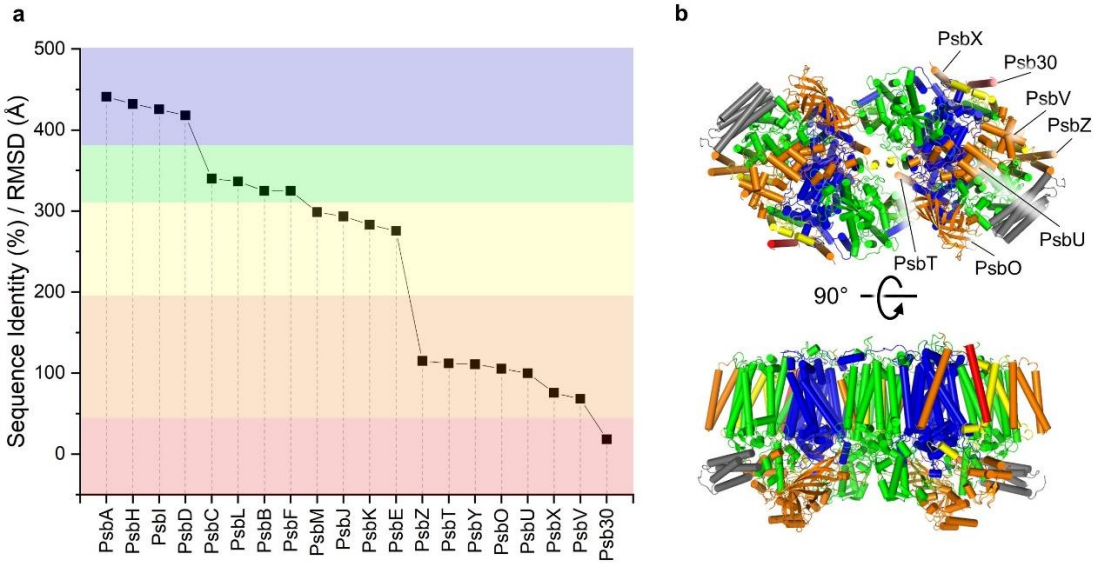

Fig. S6. Subunit similarity in *Synechocystis* 6803 PSII based on the ratio of sequence identity to the RMSD of their C_α superposition to subunits from *T. vulcanus* PSII (PDB 7D1T). **a.** Ratio of *Synechocystis* 6803 PSII subunit sequence identity to those from *T. vulcanus* calculated using Clustal Omega (15) to the RMSD of the C_α atoms of the superpositions of each subunits. For example, the sequence identity of PsbA from *Synechocystis* 6803 compared to *T. vulcanus* is 85.56% (**Table S1**) and the corresponding C_α subunit superposition RMSD is 0.194 (**Table S3**); therefore, its ratio is 441 (Y-axis). More similar subunits, based on both sequence and structure, exhibit largest values (high sequence identity with low RMSD). The subunits are listed in order of highest to lowest ratio. **b.** Subunits of the *Synechocystis* 6803 PSII structure colored according to the background colors in panel **a** showing a lumenal view (top) and a membrane plane view (bottom). Subunits with values <200 from panel **a** are labeled for one of the monomers in the lumenal view.

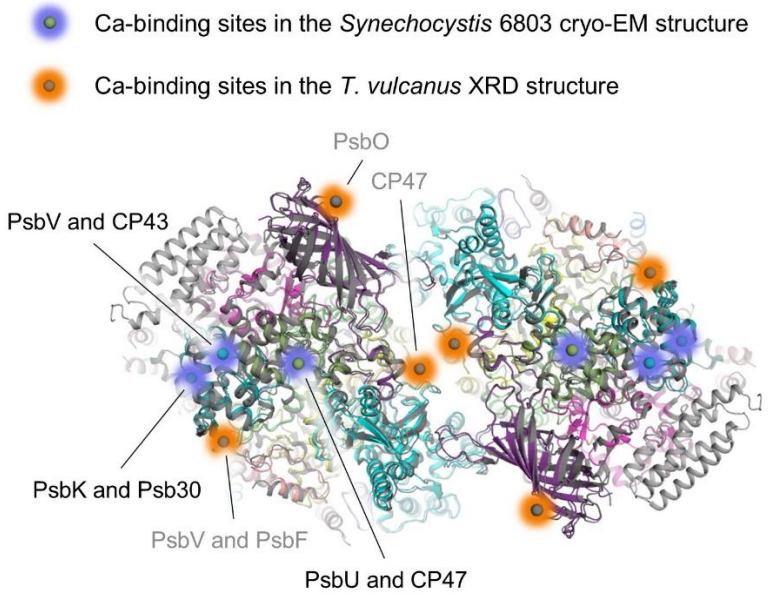

Fig. S7. Calcium-binding sites in PSII structures from *Synechocystis* 6803 and *T. vulcanus***.** A lumenal view of the *Synechocystis* 6803 cryo-EM PSII structure and the *T. vulcanus* XRD PSII structure (PDB 3WU2) are shown superimposed and the Ca-binding sites are highlighted in blue and orange, respectively. The labels denote the subunit(s) that coordinate each Ca ion. Black font pertains to Ca ions from the *Synechocystis* 6803 PSII structure and grey font pertains to Ca ions from the *T. vulcanus* PSII structure. A stromal Ca-binding site involved in crystal contacts in the *T. vulcanus* PSII XRD structure is omitted for clarity.

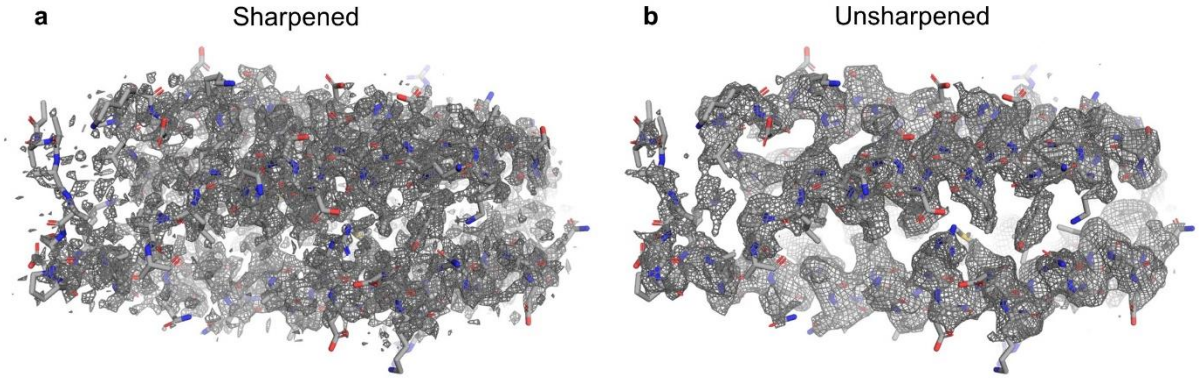

Fig. S8. Comparison of PsbQ in sharpened and unsharpened ESP maps. **a.** The PsbQ model is shown within the sharpened ESP map. **b.** The PsbQ model is shown within the unsharpened ESP map.

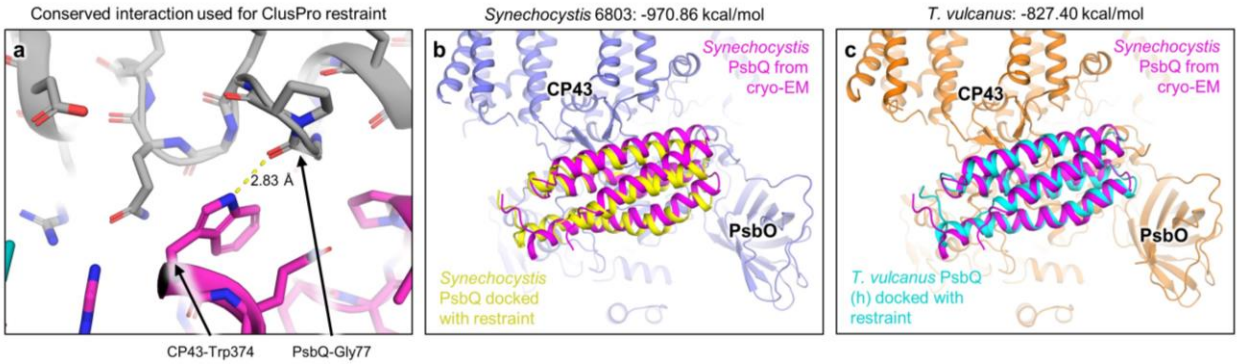

Fig. S9. Binding free energy of cyanobacterial PsbQ. **a.** The insertion of CP43-Trp374 into the broken helix of PsbQ where a H-bond is formed between the Trp sidechain indole nitrogen and the backbone carbonyl oxygen atom of PsbQ-Gly77. This interaction is conserved in the PsbQ homologs from plants and algae. Maintaining a distance of the CP43-Trp and PsbQ-Gly of <4 Å was used as the sole restraint in docking calculations. **b.** Docking calculation of *Synechocystis* 6803 PsbQ (model extracted from the *Synechocystis* 6803 PSII structure reported here), and the rest of the PSII model (created by deleting PsbQ from the model reported here). Blue ribbons show CP43 and PsbO onto which the docking was calculated. Yellow ribbons show the lowest energy cluster consensus model of docked *Synechocystis* 6803 PsbQ. Magenta shows the true location of PsbQ-binding in *Synechocystis* 6803 from the structure reported here. The PIPER ΔG calculated for this model cluster was -970.86 kcal/mol. **c.** Docking calculation of *T. vulcanus* PsbQ (homology model using the extracted *Synechocystis* 6803 PsbQ structure reported here as the template), and the PSII model from the *T. vulcanus* PSII cryo-EM structure (PDB 7D1T) where PsbQ is absent. Orange ribbons show CP43 and PsbO onto which the docking was calculated. Cyan ribbons show the lowest energy cluster consensus model of docked *T. vulcanus* PsbQ. Magenta shows the location of PsbQ-binding in *Synechocystis* 6803 from the model reported here. The PIPER ΔG calculated for this model cluster was -827.40 kcal/mol. Docking calculations were performed using the ClusPro server (12).

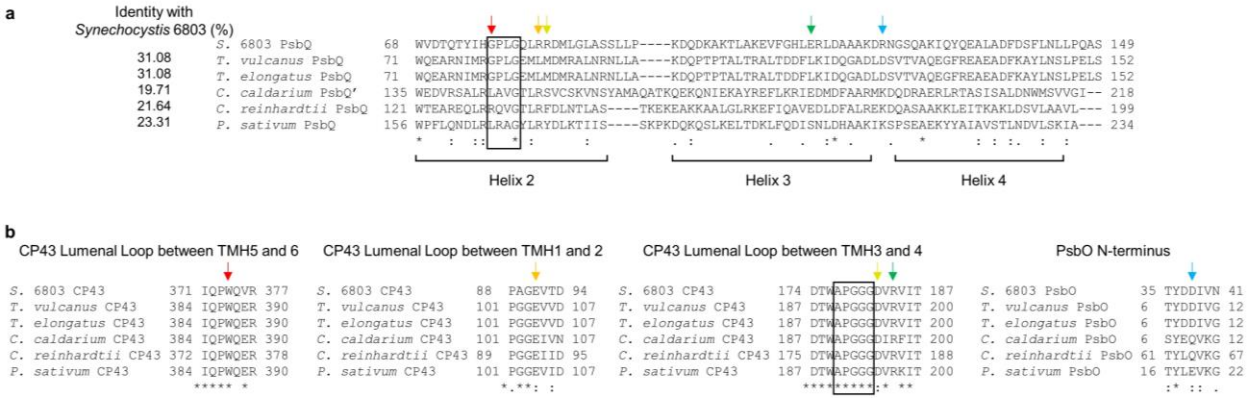

Fig. S10. Sequence alignments of residues that interact from *Synechocystis* 6803 PsbQ to other subunits in comparison with other organisms. **a.** Partial sequence alignment of PsbQ and PsbQ′ from different species. Residues in PsbQ from *Synechocystis* 6803 that interact with CP43 or PsbO are designated with an arrow. The conserved broken helix region is boxed. **b.** Partial sequence alignments of regions in CP43 and PsbO from different species. Residues that interact with PsbQQ in *Synechocystis* 6803 are designated with an arrow, colored corresponding to their interacting residue partner from panel **a**. The loop region of CP43 that inserts into the broken helix is boxed.

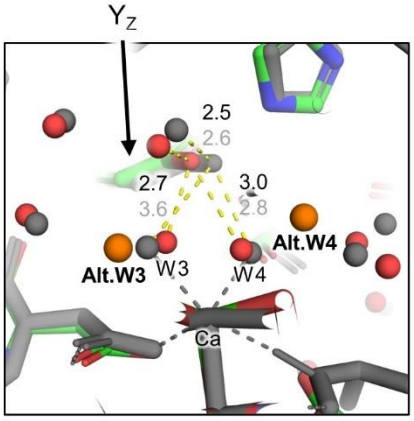

Fig. S11. H-bonding interactions of Y_Z. A superposition of the *Synechocystis* 6803 cryo-EM structure and the *T. vulcanus* XRD structure (PDB 3WU2) is shown, focused near W3 and W4. Indicated distances are shown in units of Å where those that pertain to the *Synechocystis* 6803 PSII cryo-EM structure are shown in black and the *T. vulcanus* PSII XRD structure are shown in grey. The primary and alternate positions of W3 and W4 are labeled.

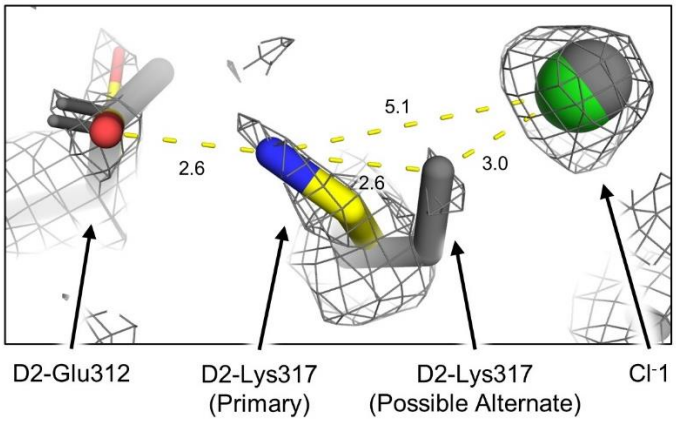

Fig. S12. Interactions of D2-Lys317. A superposition of the PSII cryo-EM structures from *Synechocystis* 6803 (PDB 7N8O) and *T. vulcanus* (PDB 7D1T) is shown, focused near D2-Lys317. The view is from a perspective near D1-Asp61. The full dose cryo-EM map from *Synechocystis* 6803 PSII is shown at 5σ. Indicated distances are shown in units of Å. The primary and possible alternate positions of the D2-Lys317 sidechain are labeled.

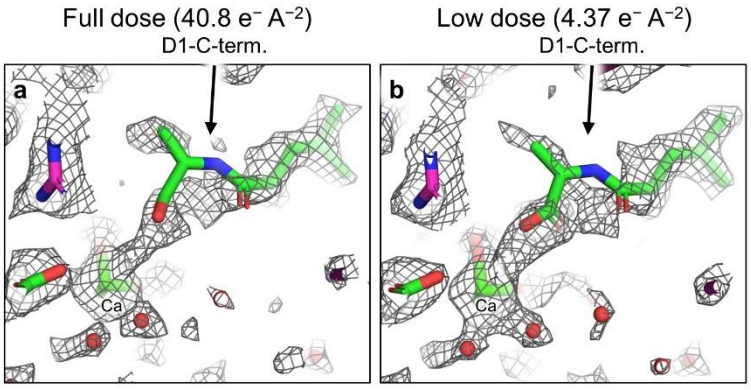

Fig. S13. Full dose and low dose ESP maps near the C-terminus of D1. **a.** Full dose map. **b.** Low dose map. In both panels, the C-terminus of D1 is shown below which the OEC is found with the Ca ion labeled for reference. Maps are shown at 6σ.

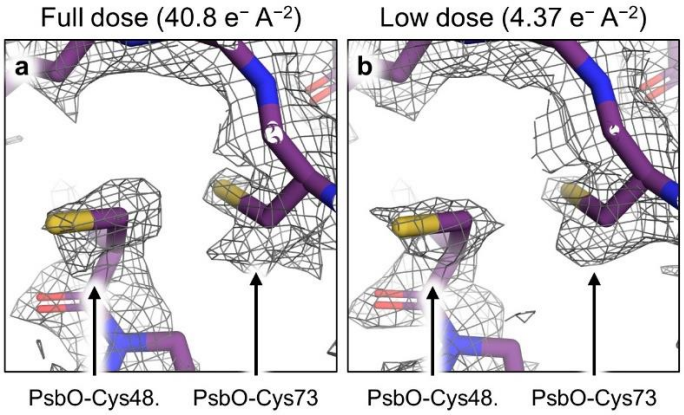

Fig. S14. Full dose and low dose ESP maps near PsbO-associated Cys residues that may form a disulfide bond. **a.** Full dose map. **b.** Low dose map. In both panels, the two Cys sidechains that could form a disulfide bond are labeled for reference. Maps are shown at 5σ.

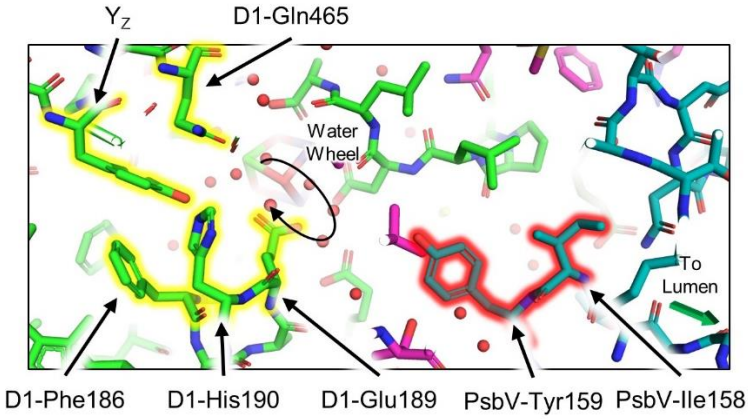

Fig. S15. Residues possibly involved in Large channel gating. The structure of *Synechocystis* PSII is shown where residues previously proposed to be involved in gating from the basis of the *T. vulcanus* PSII structure (16) are highlighted in yellow, and residues noted to be blocking the large channel and possibly involved in gating of the *Synechocystis* 6803 PSII structure are highlighted in red. The water wheel and closest entrance to the lumen are labeled.

Supplementary Tables

Table S1. Sequence identity of *Synechocystis* 6803 PSII subunits compared to those from *T. vulcanus* and *T. elongatus*.

	PsbA	PsbB	PsbC	PsbD	PsbE	PsbF	PsbH	PsbI	PsbJ	PsbK	PsbL
T. vulcanus	85.56	83.13	86.03	88.60	66.67	72.73	77.78	71.05	69.23	83.78	81.08
T. elongatus	86.11	82.64	85.43	88.35	66.67	72.73	78.12	71.05	69.23	77.78	81.08

	PsbM	PsbO	PsbQ	Psb30	PsbT	PsbU	PsbV	PsbX	PsbY	PsbZ
T. vulcanus	65.71	55.79	31.08	50.00	51.61	51.46	41.25	44.74	52.94	72.58
T. elongatus	62.86	53.70	31.08	41.30	51.61	47.29	41.25	44.74	48.72	72.58

Table S2. Cryo-EM data collection parameters and map/model statistics.

Data collection		
Magnification	x105,000	
Voltage (kV)	300	
Electron exposure (e^{-} Å^{-2})	40.8	
Images per stack	28	
Defocus range (μm)	-1.2 to -2.0	
Pixel size (Å)	0.832	
Symmetry imposed	C2	
Initial particle images (no.)	1,896,906	
Final particle images (no.)	202,844	
Processing and Refinement	**Full Dose (7N8O)**	**Low Dose (7RCV)**
Images used in processing	28	3
Dose accumulated (e^{-} Å^{-2})	40.8	4.37
Map resolution (Å)	1.93	2.01
FSC threshold	0.143	0.143
Initial model used (PDB code)	3WU2	3WU2
Model resolution (Å)	2.00	2.03
FSC threshold	0.5	0.5
Map-sharpening *B* factor (Å^2)	-33.3	-35.2
Model composition		
Non-hydrogen atoms	54,678	54,678
Protein residues	5,544	5,544
Ligands	230	230
Waters	1236	1236
B factors (Å^2)		
Protein	30.00	30.79
Ligands	28.45	42.31
Water	30.00	18.43
R.M.S. deviations		
Bond lengths (Å)	0.012	0.011
Bond angles (°)	1.502	1.434
Validation		
MolProbity	2.07	1.98
Clashscore	14.58	13.57
Rotamer outliers (%)	1.91	1.97
Ramachandran plot		
Favored (%)	96.92	97.40
Allowed (%)	3.01	2.59
Disallowed (%)	0.07	0.02

Table S3. RMSD (Å) of C_α atoms from *Synechocystis* 6803 subunits compared to those from *T. vulcanus*.

PsbA	PsbB	PsbC	PsbD	PsbE	PsbF	PsbH	PsbI	PsbJ	PsbK	PsbL
0.194	0.256	0.253	0.212	0.242	0.224	0.194	0.167	0.236	0.296	0.241

PsbM	PsbO	PsbQ	Psb30	PsbT	PsbU	PsbV	PsbX	PsbY	PsbZ
0.220	0.530	N/A*	2.719	0.416	0.515	0.605	0.592	0.477	0.631

No current structure of PSII from *T. vulcanus* maintains the PsbQ subunit.

Table S4. Sequence identity of PsbQ-related proteins from various organisms.

	***Synechocystis* 6803 PsbQ**	***T. elongatus* PsbQ**	***C. reinhardtii* PsbQ**	***C. caldarium* PsbQ′**	***P. sativum* PsbQ**	***T. vulcanus* Psb27**
***Synechocystis* 6803 PsbQ**	100.00	31.08	21.64	19.71	23.31	22.37
***T. elongatus* PsbQ**	31.08	100.00	16.79	16.31	18.25	11.84
***C. reinhardtii* PsbQ**	21.64	16.79	100.00	27.87	31.75	16.87
***C. caldarium* PsbQ′**	19.71	16.31	27.87	100.00	24.62	17.02
***P. sativum* PsbQ**	23.31	18.25	31.75	24.62	100.00	17.02
***T. vulcanus* Psb27**	22.37	11.84	16.87	17.02	17.02	100.00

Table S5. RMSD (Å) for C_α superpositions of of PsbQ-related proteins and *Synechocystis* 6803 X-ray crystal structure to the *Synechocystis* 6803 cryo-EM PsbQ structure.

Synechocystis* 6803 PsbQ (X-ray)	***T. elongatus* PsbQ (X-ray)***	***C. reinhardtii* PsbQ (cryo-EM)**	***C. caldarium* PsbQ′ (X-ray)**	***P. sativum* PsbQ (cryo-EM)**	***T. vulcanus* Psb27 (cryo-EM)**
0.397	1.148	1.075	1.278	1.102	6.225

*Structure determined of the purified subunit not associated with the core complex.

Table S6. Calculated free energy of PsbQ-binding in cyanobacteria. Calculations were performed using ClusPro (12). PIPER energy units are reported in kcal/mol.

ClusPro Weighting Coefficient Set	***Synechocystis* 6803**	***T. vulcanus***
Balanced	-816.52	-724.85
Electrostatic-favored	-970.86	-827.4
Hydrophobic-favored	-781.35	-589.15
VdW+Elec	-236.49	-148.6

Table S7. Calculated Mulliken spin densities and oxidation state assignments for Mn ions in *Synechocystis* 6803 PSII.

	Initial oxidation state (Mn1-Mn4)	Mn1	Mn2	Mn3	Mn4	Final oxidation state (Mn1-Mn4)
Initial Guess 1 (S=7)	III, IV, IV, III	4.74	4.28	4.19	4.85	II, III, III, II
Initial Guess 2 (S=0)	III, IV, IV, III	4.60	-4.38	4.09	-4.89	II, III, III, II
Initial Guess 3 (S=0)	II, II, II, II	4.81	-4.78	4.36	-4.27	II, II, III, III

Table S8. PsbV C-terminal region sequence comparison and associated organismal growth temperatures.

Organism	Approximate growth temperature (°C)*	C-terminal sequence alignment of PsbV
Synechocystis sp. PCC 6803	36 (17)	WGGT-IYF
Synechocystis salina LEGE 06155	25 (18)	WGGT-IYF
Synechocystis sp. PCC 6714	28 (19)	WGGT-IYF
Snowella sp.	20 (20)	WGGT-IYF
Microcystis aeruginosa	23 (21)	WGGT-IYF
Prochlorococcus marinus	24 (22)	WGGGKIYF
Halomicronema hongdechloris	32 (23)	WASGKPGR
Trichodesmium erythaeum	26 (24)	WGGGKIFR
Acaryochloris marina	25 (25)	WGGGKANR
Cyanothece sp. PCC 7425	30 (26)	WGGGKIYF
Nostoc punctiforme	3 (27)	WGGGKIYY
Leptolyngbyaceae cyanobacterium JSC-12	45 (28)	WGGGKIYY
Thermosynechococcus elongatus	57 (29)	WGGGKVYY
Thermosynechococcus vulcanus	57 (29)	WGGGKVYY

*Based on reference.

Table S9. Metal-metal distances of the OEC in selected PSII structures. All measurements are taken from monomer A of the published coordinates and all values are reported in Å. Radiation dose was converted to MGy, although it should be noted that radiation damage corresponding to different radiation types may not be comparable.

	***S.* 6803 Cryo-EM 151 MGy PDB 7N8O**	***S.* 6803 Cryo-EM 16.2 MGy PDB 7RCV**	***T. vulcanus* Cryo-EM 307 MGy PDB 7D1T**	***T. vulcanus* Cryo-EM 12.2 MGy PDB 7D1U**	***T. vulcanus* X-ray 0.03 MGy PDB 5B5E**	***T. elongatus* X-ray N/A* PDB 6W1O**
Mn1-Ca	3.76	3.85	3.52	3.57	3.51	3.40
Mn1-Mn2	3.13	3.07	2.83	2.87	2.74	2.81
Mn1-Mn3	3.41	3.44	3.36	3.20	3.22	3.29
Mn1-Mn4	5.07	5.23	5.02	5.09	4.91	4.81
Mn2-Ca	3.58	3.58	3.45	3.43	3.35	3.43
Mn2-Mn3	3.05	2.98	3.10	2.88	2.76	2.94
Mn2-Mn4	5.66	5.75	5.65	5.46	5.22	5.28
Mn3-Ca	3.42	3.44	3.29	3.45	3.39	3.47
Mn3-Mn4	2.95	3.12	2.97	3.03	2.82	2.67
Mn4-Ca	3.86	3.93	3.69	3.76	3.75	3.85
Mean Mn-Mn	**3.88**	**3.93**	**3.82**	**3.76**	**3.61**	**3.63**

*The structure was determined using an X-ray free electron laser and thus data were hypothetically collected before the onset of radiation damage.

References

1. Q. Wang, S. Yang, S. Wan, X. Li, The significance of calcium in photosynthesis. *Int. J. Mol. Sci.* **20**, 1353 (2019).
2. A. K. Hochmal, S. Schulze, K. Trompelt, M. Hippler, Calcium-dependent regulation of photosynthesis. *Biochim. Biophys. Acta - Bioenerg.* **1847**, 993–1003 (2015).
3. C. F. Yocum, The calcium and chloride requirements of the O_2 evolving complex. *Coord. Chem. Rev.* **252**, 296–305 (2008).
4. K. Kato, *et al.*, High-resolution cryo-EM structure of photosystem II reveals damage from high-dose electron beams. *Commun. Biol.* **4**, 382 (2021).
5. Y. Umena, K. Kawakami, J.-R. Shen, N. Kamiya, Crystal structure of oxygen-evolving Photosystem II at a resolution of 1.9 Å. *Nature* **473**, 55–60 (2011).
6. J. W. Murray, J. Barber, Identification of a calcium-binding site in the PsbO protein of photosystem II. *Biochemistry* **45**, 4128–4130 (2006).
7. A. Guskov, *et al.*, Cyanobacterial photosystem II at 2.9-Å resolution and the role of quinones, lipids, channels and chloride. *Nat. Struct. Mol. Biol.* **16**, 334–342 (2009).
8. S. A. Jackson, R. D. Fagerlund, S. M. Wilbanks, J. J. Eaton-Rye, Crystal structure of PsbQ from *Synechocystis* sp. PCC 6803 at 1.8 Å: Implications for binding and function in cyanobacterial photosystem II. *Biochemistry* **49**, 2765–2767 (2010).
9. F. Michoux, *et al.*, Crystal structure of CyanoQ from the thermophilic cyanobacterium *Thermosynechococcus elongatus* and detection in isolated photosystem II complexes. *Photosynth. Res.* **122**, 57–67 (2014).
10. A. D. Juneau, L. K. Frankel, T. M. Bricker, J. L. Roose, N-terminal lipid modification is required for the stable accumulation of CyanoQ in *Synechocystis* sp. PCC 6803. *PLoS One* **11**, e0163646–e0163646 (2016).
11. H. Ago, *et al.*, Novel features of eukaryotic photosystem II revealed by its crystal structure analysis from a red alga. *J. Biol. Chem.* **291**, 5676–5687 (2016).
12. D. Kozakov, *et al.*, The ClusPro web server for protein–protein docking. *Nat. Protoc.* **12**, 255–278 (2017).
13. J. Zivanov, *et al.*, New tools for automated high-resolution cryo-EM structure determination in RELION-3. *eLife* **7**, e42166 (2018).
14. P. D. Adams, *et al.*, PHENIX: A comprehensive python-based system for macromolecular structure solution. *Acta Crystallogr. Sect. D Biol. Crystallogr.* **66**, 213–221 (2010).
15. F. Sievers, *et al.*, Fast, scalable generation of high quality protein multiple sequence alignments using Clustal Omega. *Mol. Syst. Biol.* **7**, 1–6 (2011).
16. F. M. Ho, Uncovering channels in photosystem II by computer modelling: Current progress, future prospects, and lessons from analogous systems. *Photosynth. Res.* **98**, 503 (2008).
17. T. Zavřel, M. A. Sinetova, D. Búzová, P. Literáková, J. Červený, Characterization of a model cyanobacterium *Synechocystis* sp. PCC 6803 autotrophic growth in a flat-panel photobioreactor. *Eng. Life Sci.* **15**, 122–132 (2015).
18. A. L. Gonçalves, *et al.*, Co-cultivation of *Synechocystis salina* and *Pseudokirchneriella subcapitata* under varying phosphorus concentrations evidences an allelopathic competition scenario. *RSC Adv.* **6**, 56091–56100 (2016).
19. D. Kamravamanesh, *et al.*, Photosynthetic poly-β-hydroxybutyrate accumulation in unicellular cyanobacterium *Synechocystis* sp. PCC 6714. *AMB Express* **7**, 143 (2017).

20. P. Rajaniemi-Wacklin, *et al.*, Correspondence between phylogeny and morphology of *Snowella* spp. and *Woronichinia naegeliana*, cyanobacteria commonly occuring in lakes. *J. Phycol.* **42**, 226–232 (2006).
21. S. Missaghi, M. Hondzo, C. Sun, M. Guala, Influence of fluid motion on growth and vertical distribution of cyanobacterium *Microcystis aeruginosa*. *Aquat. Ecol.* **50**, 639–652 (2016).
22. E. R. Zinser, *et al.*, Influence of light and temperature on *Prochlorococcus* ecotype distributions in the Atlantic Ocean. *Limnol. Oceanogr.* **52**, 2205–2220 (2007).
23. Y. Li, Y. Lin, P. Loughlin, M. Chen, Optimization and effects of different culture conditions on growth of *Halomicronema hongdechloris* – A filamentous cyanobacterium containing chlorophyll *f*. *Front. Plant Sci.* **5**, 67 (2014).
24. T. G. Boatman, T. Lawson, R. J. Geider, A key marine diazotroph in a changing ocean: The interacting effects of temperature, CO_2 and light on the growth of *Trichodesmium erythraeum* IMS101. *PLoS One* **12**, e0168796–e0168796 (2017).
25. R. S. Gloag, R. J. Ritchie, M. Chen, A. W. D. Larkum, R. G. Quinnell, Chromatic photoacclimation, photosynthetic electron transport and oxygen evolution in the chlorophyll d-containing oxyphotobacterium *Acaryochloris marina*. *Biochim. Biophys. Acta - Bioenerg.* **1767**, 127–135 (2007).
26. C. Chenebault, *et al.*, A genetic toolbox for the new model cyanobacterium *Cyanothece* PCC 7425: A case study for the photosynthetic production of Limonene. *Front. Microbiol.* **11**, 2335 (2020).
27. B. Thangaraj, *et al.*, Cytomorphological and nitrogen metabolic enzyme analysis of psychrophilic and mesophilic *Nostoc* sp.: a comparative outlook. *3 Biotech* **7**, 107 (2017).
28. B. Igor, *et al.*, High-quality draft genome sequence of the siderophilic and thermophilic *Leptolyngbyaceae cyanobacterium* JSC-12. *Microbiol. Resour. Announc.* **10**, e00495-21 (2021).
29. K. Onai, M. Morishita, S. Itoh, K. Okamoto, M. Ishiura, Circadian rhythms in the thermophilic cyanobacterium *Thermosynechococcus elongatus*: Compensation of period length over a wide temperature range. *J. Bacteriol.* **186**, 4972–4977 (2004).